JOURNAL OF PROPULSION AND POWER
Vol. 23, No. 6, November–December 2007

Experimental Investigation of Waterhammer in Simplified Feed Lines of Satellite Propulsion Systems

Renaud Lecourt*
ONERA, 31410 Mauzac, France
and
Johan Steelant†
ESA, 2200 AG Noordwijk, The Netherlands

DOI: 10.2514/1.29269

Operation of spacecraft propulsion systems is regularly adversely faced with waterhammer. The presence of very low pressures or vacuum complicate the classically known waterhammer due to various multiphase phenomena such as cavitation, absorption and desorption of a pressurizing gas, boiling, etc. This complex behavior is hard to model due to a lack of understanding of the physical processes taking place. To build up an experimental database on waterhammers in multiphase confined environments for validation of physical models, a literature survey was first undertaken on detailed waterhammer experiments. Only a few papers with well-documented experiments were found. None of the experiments found matched all the specifications needed for proper simulation and validation in satellite and spacecraft hardware and physical configurations. To complement the literature database, a detailed experimental investigation of the waterhammer phenomenon in a confined environment was required. This investigation was carried out using a simplified setup with two inert fluids, ethanol and acetaldehyde, and an actual propellant, monomethylhydrazine. Numerous tests were performed that confirmed excellent reproducibility of the results. The experiments showed that ethanol can be used instead of toxic monomethylhydrazine for estimating the waterhammer amplitude. The initial pipe pressure has a great influence on the waterhammer amplitude, but it would appear that the fluid vapor pressure is not a physical boundary with respect to waterhammer characteristics. The waterhammer phenomenon produced in a pipe with a low initial pressure exhibited a complex evolution over time and slight differences in amplitude and features according to the pipe geometry.

Nomenclature

A	=	cross section, m^2
Cp	=	heat capacity, J/kg/K
c	=	velocity of sound, m/s
K	=	modulus of elasticity, Pa
Lv	=	latent heat, J/kg
P	=	pressure, Pa
Pv	=	vapor pressure, Pa
T	=	temperature, K
V	=	volume, m^3
v	=	velocity, m/s
λ	=	conduction coefficient, W/m/K
μ	=	viscosity, Pa · s
ρ	=	density, kg/m^3
σ	=	surface tension, N/m

Subscripts

c	=	cavity or critical point
f	=	front plane
g	=	gas
l	=	liquid phase
sw	=	stress wave
vap	=	vapor phase
wh	=	waterhammer

Received 12 December 2006; revision received 5 June 2007; accepted for publication 22 June 2007.

*Research Engineer, Department for Aerodynamics and Energetics, Centre du Fauga-Mauzac.

†Research Engineer, European Space Research and Technology Centre, Division of Propulsion and Aerothermodynamics, Keplerlaan 1. Member AIAA.

I. Introduction

PRODUCING thrust in a rocket engine, priming feeding lines, or venting reservoirs into space results in the expelling of a fluid from a reservoir to the ambient (i.e., space) vacuum. This induces a flow or a spray in which multiphase aspects play a key role in the physical fluid behavior. In space systems, satellites, or interplanetary probes, the propellant lines are vacuum-pumped or filled with low-pressure helium or nitrogen before the launch. Before operations, these lines are primed with a vaporizing liquid, sometimes in the presence of a noncondensable gas (NCG), which produces waterhammer phenomena. These phenomena occur regularly in aerospace applications. Other examples are fuel injectors in diesel engines or gas turbines, fire sprinklers, water hoses, etc. From the moment a valve is opened, the quick filling of the lines produces a shock wave (waterhammer), which travels through the feed lines, inducing pressure peaks and frequencies that can either lead to equipment failure or to the excitation of system resonances. The frequency is related to the velocity of sound c, whereas the pressure peak is also determined by the density ρ_l and the final liquid front velocity $v_{l,f}$ by $P_{\text{wh}} = \rho_l \cdot c \cdot v_{l,f}$.

The combined action of two components (e.g., a liquid propellant and a pressurizing gas) alters the sound velocity of the compound fluid, which, depending on the relative volume fraction, may be significantly lower than the relative sound velocity of the individual components. This large variation alters the amplitude of the waterhammer and its frequency and damping characteristics. Concurrently, a pressurizing gas can be absorbed or desorbed in the liquid propellant at a finite rate, which also affects the effective velocity of sound. Finally, during the transient phase, the presence of areas with a lower pressure than the vapor pressure may cause unsteady cavitation pockets followed by an implosion when a pressure wave flows over them.

Predicting or simulating this complex multiphase and unsteady behavior is of obvious importance both for designing propulsion

systems and for analyzing in-flight anomalies and postflight data. To enable this, the various physical phenomena need to be understood and, accordingly, the models require validation with data from a coherent database of experiments.

Little consistent information and data that are applicable to the envisaged phenomena and applications are available, as will be discussed in the next section. Hence, as an initial step toward its modeling, a logical requisite is to establish this waterhammer database for two-phase, two-component flows applicable to propulsion systems for both spacecraft and launchers, which will be discussed in Secs. III and IV.

II. Literature Survey

The literature was reviewed to obtain information on the physics of phenomena related to waterhammers and to record well-documented experiments, which could then be used to validate computational fluid dynamics (CFD) physical multiphase models. The experiments chosen for the database must therefore reproduce, as far as possible, a waterhammer phenomenon with vaporization, cavitation, and recondensation of the liquid involved with a variable fraction of noncondensable gas.

Computer simulation of experimental results requires accurate knowledge of boundary and initial conditions, requiring inclusion of well-documented and accurate descriptions of 1) the setup, 2) the measurement transducers and acquisition system, 3) the experimental procedure, and 4) the experimental measurements.

It appears that few papers have dealt solely with the waterhammer phenomenon. The principal concern of researchers and users of hydraulic systems is to determine the fluid–structure interaction to avoid structural failures. For a lot of the experiments, many stress or acceleration measurements were taken on the structure, whereas few pressure measurements were taken on the liquid side. Moreover, many papers deal with theoretical and computational developments. A few papers describing the waterhammer phenomenon in actual space propulsion systems are hardly of any use because the hardware is too complex and not well-documented. Finally, experimental study of the waterhammer phenomenon requires transducers with a large bandwidth and high-rate acquisition systems. Consequently, papers on experiments that are too old do not produce workable results.

Although it does not describe an actual experiment, [1] is very interesting because it is a thorough review of what had been done on fluid–structure interaction up to 1996. This paper gives a good description of the phenomena and quotes the best experimental works. Generally, a waterhammer is not only a pressure wave traveling in a liquid at sound velocity. When there is interaction with the structure, three additional mechanisms may be observed: friction coupling, Poisson coupling, and junction coupling. *Friction coupling* represents the mutual friction between liquid and pipe. The more significant *Poisson coupling* is due to a radial expansion of the pipe induced by pressure in the fluid, which in turn induces a pipe radial contraction downstream through a traveling axial stress. The pipe radial contraction itself causes an increase of pressure in the fluid. This axial stress travels at sound velocity in the metal, which is often greater than sound velocity in the fluid, and Poisson coupling leads to precursor waves in the fluid, which travel in front of the waterhammer wave. Friction coupling and Poisson coupling act along the entire pipe. *Junction coupling* acts at specific points in a pipe system, such as bends, T-junctions, etc.

The author also points out that to produce useful experimental results for theoretical or numerical validation, the experiments have to be performed with suspended tubes. The waterhammer is obtained by hitting one extremity of the tube with a pendulum rod. This way, the initial conditions (i.e., energy transmitted to the tube: liquid and structure) and the boundary conditions are well-known. In a setup with a valve, the operation of the valve is never accurately known.

These preceding remarks first mean that if the software code does not take Poisson and junction couplings into account, the validation experiments for the waterhammer module must involve experimental setups that are as rigid as possible. Second, the opening conditions of the valve will have to be known as well as possible. Third, the boundary conditions and the setup will have to be as simple as possible.

This review [1] was updated in a paper [2] focused on fluid–structure interaction in flexible piping and in a paper [3] published in 2006. The second reference [2] was not considered because it seemed too far from the purpose of the present work, and the third reference [3] was published too late to be considered.

From this first literature reference [1], only seven papers were selected for the database, four of them describing experiments in impacted pipes [4–7] and four [7–10] with a setup including a valve. The other references were discarded either because they were not well-documented or because the experimental setup did not meet the present requirements for simplicity or clean and well-known boundary conditions. A short description of each of these papers is given subsequently, showing how the experiments inspired the one used in the present study and giving guidelines to readers who are interested in how to validate a two-phase waterhammer model.

The experiments in [4] were performed with a straight pipe hit by a pendulum rod. The steel pipe is filled with water. The liquid is stored in the pipe at several different pressure levels, from 0.1 to 2 MPa, so that at lower levels, the rarefaction wave, produced by the reflection of the compression wave at the end of the pipe, induces cavitation in the liquid. The characteristics of the setup, as well the experimental conditions, are well-documented and the experimental results are useful for CFD validation, although the original graphics are somewhat small. The graphics in [4] display the pressure and vapor cavity volume (v, cm^3) vs time at the ends of the pipe for the five sets of experimental conditions described. They also compare the experimental results with numerical ones from two models. The experiments are ranked by a severity index S based on the axial-stress wave speed c_{sw}, the length L, and the duration of the first vapor cavity T_c:

$$S = \frac{T_c}{(2L/c_{\mathrm{sw}})} \tag{1}$$

In [5], the experiment used the same setup as the previous reference [2], except that the remote end was replaced by an elbow and a short straight-pipe section. The setup and the experiments are again well-documented. Four experiments are described in the paper. The only parameter is the initial fluid pressure in the pipe, which either induces cavitation or does not. The original graphics are larger than in the previous reference and therefore more readable. They display the fluid pressure vs time downstream from the elbow at the remote end of the pipe and the axial pipe velocity vs time at the impact end.

Reference [6] was published by the same team as the previous papers and a similar experimental setup was used (i.e., the same impacting rod and pipes). The paper describes two kinds of experiments: one with the straight pipe used in [4] and one with a T-junction pipe. The experiments are not as well-documented as for the previous papers. For example, the initial conditions are not given and the pressure measurements appear to be relative measurements. If this information can be deduced from the experimental results, then the paper is of interest for validating CFD tools, because the numerical values are given for some curves. Reference [7] also describes two setups. The first one is of a pipe, filled with liquid, hit by a rod to produce the waterhammer. The pipe is made of steel, and two fluids (water and oil) were used. The setup and the experiment are not fully documented. For example, the internal length of the pipe is not known. However, because the purpose of the experiment was to investigate the propagation of a pressure pulse along the pipe before its reflection at the remote end according to the fluid viscosity, it should be adequate for CFD validation. The paper displays the experimental results of the pulse propagation for two liquids with different viscosity and two pulse amplitudes.

The second experiment used a setup composed of a reservoir emptying itself through a pipe with a rapid-closure valve at the end of the pipe. The pipe was made of copper and imbedded in concrete to avoid fluid–structure interaction. Water and oil were also used, as in the previous experiment. Once again, the setup and the experiment

are not fully documented, but appear to give all the useful information. The experimental results are displayed in nondimensional units and relate changing pressures to time at two different locations of the pipe for both liquids with different viscosities. The large dimensions of the experiment apparatus might be a drawback. Reference [8] also deals with the discharge of a reservoir through a pipe with a waterhammer produced by the rapid closure of a valve. The pipe was made of steel and the fluid was water. The purpose of this work was to measure reflection and transmission coefficients of bends crossed by pressure pulses. These measurements were then used to elaborate correlations that give the coefficient value according to the geometrical and material characteristics of the bend. A large number of parameters were investigated: fluid flow velocity, pipe material, bore-to-thickness ratio, applied restraints on the bends, and geometrical characteristics of the bends. The graphics display, in physical units, the amplitude of the transmitted, and the reflected wave vs the steady fluid velocity before the valve closure, according to an increasing restraint placed on the pipeline and the bend. The curves show that the last parameter had no influence; the setup was certainly rigid enough, no matter what the restraint.

The work covered in [9] is not very well-documented, but it has the advantage of dealing with a fluid (kerosene) that is assumed to be saturated with air. The setup is a closed loop, composed of two tanks, connected in parallel by a pipe with a rapid-closure valve and by a circuit including a pump and a venturi on the pipe. The system considered by the author consists of the pipe and tank downstream from the valve. The dimensions are large (the pipe with the valve is 70 m long). Four experiments are described, with the initial fluid pressure and steady velocity as parameters. The kerosene is assumed to be saturated with air, but there is no indication of the actual amount of air dissolved in it. The experimental results are displayed as pressure downstream from the valve vs time, once the valve has been closed. We should note that the accurate location of the transducer is not given; it should be close to the valve.

The last work [10] is also of the tank-pipe-valve type. The experiment corresponds to a classical waterhammer phenomenon: a valve is quickly closed to stop a flow. The setup is fairly well-documented. The pipe is made of steel. Some indications are given as to the actual sound velocity of water during the experiments. It was measured through the frequency of the quarter-wave acoustic mode of the pipe, but a lower value had to be used for the computations performed to reproduce the experiments. The authors also provide information on the closure of the valve. They measured the steady loss coefficient according to the valve angle, then, assuming that the loss coefficient values were valid for transition phases and combining the valve angle vs time curve, they obtained a nondimensional valve opening vs time parameter to describe the transient closure of the valve. The experimental results consist of pressure measurements vs time at well-defined locations.

We may conclude the literature survey by noting that only a few papers were found that described well-documented experiments with setups that were rigid enough to avoid too many fluid–structure interactions. In these papers, two kinds of setup were described: 1) pipes filled with liquid and hit by a pendulum rod and 2) assemblies consisting of tank pipes with rapid-closure valves.

The experiments performed on the first setups are very well-documented and with well-known boundary and initial conditions. They reproduce waterhammer and cavitation phenomena, but without the two-component flows found in a spacecraft propellant system (i.e., downstream from a valve and with a noncondensable gas).

The second setups are similar to spacecraft propellant systems, and the experiments reproduce a waterhammer, but without the presence of cavitation or two-component, two-phase flow. Moreover, the valve closure transient is not very well-documented, which is a large drawback for CFD validation. These experiments can only be used for partial validation of a software module dealing with a waterhammer combined with two-phase flow. Consequently, the experimental investigation of the waterhammer phenomenon typical for spacecraft systems was decided upon and is discussed in the next section.

III. Experimental Setup

A. Setup

The setup was designed to reproduce, in a simplified way, a spacecraft liquid propulsion system, from the pressurizing system to the injection valve of a rocket engine. An additional vacuum system is added to set the system's initial conditions. It was derived from a former setup used to measure waterhammer amplitudes with monomethylhydrazine (MMH) and nitrogen tetroxide (NTO) propellants in simple feed-line elements [11]. As described in Fig. 1, the setup consists of 1) a pressurizing and depressurizing system with valves V1 and V2, 2) a propellant tank with an isolation valve MV4, 3) a nitrogen purge system closed by valve V5, 4) a vacuum system with an isolation valve V8, 5) the fast-opening valve V7, 6) the element to be tested, and 7) at the downstream end of the element, a measurement module [11], closed with a plug.

In the similarity between the experimental setup and a spacecraft liquid propulsion system, the plug replaces the injection valve in a rocket engine and will sustain the same waterhammer effects as those during the priming of the propulsion system. The test pipe was supported by four rigid legs with clamp collars. The tank is cylindrical with flat ends. Its internal diameter is 135 mm. The circuit between the tank and the fast-opening valve is fairly complex. From the tank, there are first three successive 250-mm-long 90-deg rounded bends, the manual valve MV4, and then a 490-mm-long (including valve length) straight pipe. The internal diameter of the elements is 20 mm. Then after a reduction and the manual valve MV6, the pipe consists successively of an 80-mm-long 90-deg rounded bend, a 400-mm straight pipe, another 80-mm-long 90-deg rounded bend, and a 100-mm-long straight circuit up to the ball valve V7. The internal diameter of this second circuit part is 10 mm. The total length of the circuit upstream from the test section is therefore about 1900 mm.

Full opening of the fast ball valve takes between 25 and 30 ms. From its geometric characteristics (ball diameter of 21.9 mm, ball-orifice diameter of 9.9 mm, and sealing-orifice diameter of 11.5 mm), it may be estimated that its opening begins at an angle of 31.4 deg and ends at 85.2 deg. It is also possible to compute the evolution of the relationship between the opened section vs the opening angle and compare the result with the pipe section (about 24 mm^2) to evaluate the time when the "valve-opened" section is larger than the pipe section (i.e., when the opening of the valve has no more influence on the acceleration of the liquid in the pipe). Finally, the experimental results described in Sec. IV show that the *efficient* opening time of the ball valve was short enough, compared with the transit time and therefore to the acceleration phase of the liquid in the pipes, to obtain high-amplitude waterhammers.

Two pipe elements were tested: one 2 m long and straight and another 2 m long and bent at 90 deg at midlength. Both the pipes had an outer diameter of 6.35 mm and a 0.41-mm wall thickness. They were made of titanium alloy (TA3V). Their accurate geometric characteristics are shown in Table 1 and other details can be found in [11].

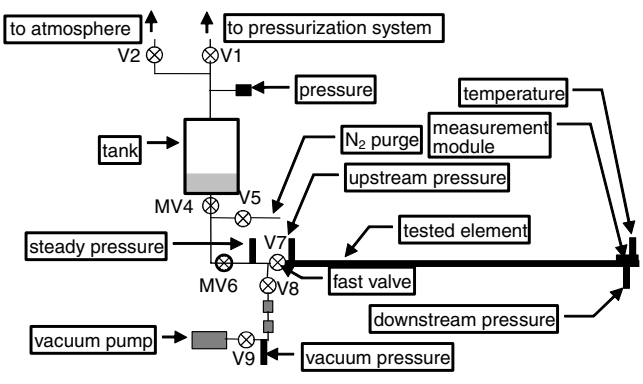

Fig. 1 Experimental setup.

Table 1 Pipe configurations

	Straight pipe	Bent pipe
Valve/$P_{upstream}$ distance, mm	70	70
$P_{upstream}/P_{downstream}$ distance, mm	2000	2090
$P_{upstream}$/bent distance, mm	——	1035
Curvature radius, mm	——	35
Bent/$P_{downstream}$ distance, mm	——	1000
$P_{downstream}$/plug distance, mm	40	40
Inner diameter, mm	5.53	5.53
Wall thickness, mm	0.41	0.41
Material	TA3V	TA3V

B. Instrumentation

The instrumentation can be divided into two groups: dedicated instrumentation for setting the experiment parameters and instrumentation for recording the waterhammer phenomenon.

The first instrumentation group consisted of (Fig. 1) 1) a steady-state tank pressure transducer to set the required tank pressure value; 2) a steady-state pipe pressure transducer to set the right pressure parameter for the noncondensable gas in the pipe as equal to or greater than 1 atm; 3) a steady-state vacuum pressure transducer to check the vacuum level and set the noncondensable-gas pressure value in the pipe at less than 1 atm; 4) a thermocouple to measure the ambient temperature, which is also the propellant temperature before the experiment; and 5) an ultrasonic transducer to measure the sound velocity of the fluid in the tank before the experiment.

The second instrumentation group consisted of 1) a downstream unsteady pressure transducer and 2) a thermocouple.

The transducers were installed in the measurement module (Fig. 1) to measure these parameters during generation of the waterhammer. The downstream pressure transducer was flush-mounted 40 mm upstream from the plug, and the thermocouple protruded into the module cavity 13 mm upstream from the plug (Fig. 2). Finally, on the pipe, close to the fast-opening valve (Fig. 1), an upstream unsteady pressure transducer was used to detect the waterhammer wave traveling back to the tank, allowing the determination of the wave velocity between the two unsteady pressure transducers. This upstream pressure transducer was mounted on an adaptor, welded in a recess away from the pipe.

Except for the ultrasonic transducer, which was operated with its own electronics, all these measurements were digitally acquired at a frequency of 40 kHz. This acquisition rate is coherent with the unsteady pressure transducers (piezoelectric Kistler 601H), which have a resonant frequency of 130 kHz.

C. Test Procedure and Matrix

The first step in the test procedure was the tank pressurization to let the pressurizing gas reach its thermal equilibrium before the experiment. Then a rough vacuum (about 0.01 MPa) was created in the pipe volume between MV4 and V7 (see Fig. 1). After the MV6 valve was closed and the volume between valves MV4, MV6, and V5 was filled with liquid, the circuit was vacuum-pumped and then filled with nitrogen if necessary, until the targeted P_{pipe} value was reached, followed by the closure of the valve V7. It should be noted

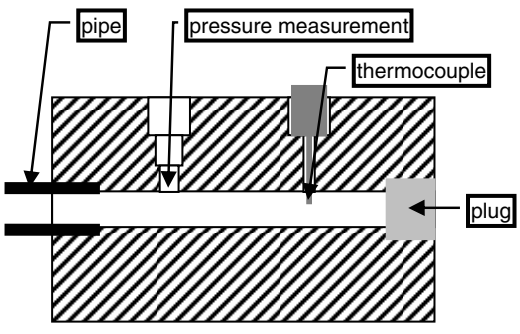

Fig. 2 Measurement volume.

Table 2 Inert fluid and propellant physical properties at 280 K

Fluid	Ethanol	MMH	Acetaldehyde	NTO
		Liquid phase		
ρ_l, kg/m^3	800.3	885.8	783.4	1476.4
Cp_l, J/kg/K	2392	2749	2469	1530
μ_l, Pa · s	0.00148	0.00110	0.000254	0.000504
λ_l, W/m/K	0.173	0.251	0.194	0.145
σ (N/m)	0.0222	0.0356	0.0205	0.0287
Lv , J/kg	1,005,800	905,600	612,000	395,400
Pv, Pa	2547	2220	59,260	51,640
Pv at 293 K, Pa	5816	4940	99260	95830
c, m/s	1279	1631	——	1058
P_c, MPa	6.14	8.24	5.57	10.13
T_c, K	513.9	567	466	430.9
		Vapor phase		
ρ_{vap}, kg/m^3	0.050	0.044	1.121	2.041
Cp_{vap}, J/kg/K	1354	1513	1272	836
μ_{vap}, Pa · s	$7.99\ 10^{-6}$	$7.36\ 10^{-6}$	$6.96\ 10^{-6}$	$2.14\ 10^{-5}$
λ_{vap}, W/m/K	0.0126	0.0108	0.0105	0.0203

that because of the limited performance of the vacuum pump, "vacuum" means a P_{pipe} pressure value between 0.5 and 1 kPa. Finally, after emptying the pipe section between the MV6 and V7 valves, V8 was closed and MV6 was opened to fill the circuit between MV6 and V7 with liquid. If necessary, the tank pressure was adjusted, after which the setup was ready for the experiment.

The experiment was triggered by opening valve V7. The pressurized liquid surged into the pipe up to the measurement module and the pipe end plug. The waterhammer was produced by the impact of the liquid on the end plug. After the impact, the compression wave traveled back and forth from the end pipe plug to the tank, damping over time. Because the objective of the study was to determine the relation between two-phase flow phenomena and the maximum waterhammer pressure, we focused our investigations on the pressure rise at the first impact of the liquid on the pipe end plug.

Finally, after the experiment, the tank was isolated (with MV4 closed), the pipe end plug was unscrewed, and the liquid was purged by flowing nitrogen from valve V5 through the pipe.

For safety reasons, it was decided to perform the main part of the experiments with inert fluids (ethanol instead of MMH and acetaldehyde instead of NTO) as the actual propellants. These fluids have fairly similar physical properties (see Table 2), especially for vapor pressure, latent heat of vaporization, and surface tension, which were considered as primary parameters at the beginning of the study. For the most interesting configurations, some tests with MMH were planned, allowing comparison with the ethanol tests. It was decided not to do tests with NTO, because this corrosive fluid is highly volatile and therefore difficult to handle safely. Furthermore, such tests with NTO have already been performed with almost the same hardware [11].

The protocol required that the parametric study include the following items: 1) influence of the P_{tank}/P_{pipe} ratio (several values), 2) influence of cavitation occurrence (this means a high P_{tank}/P_{pipe} ratio value), and 3) influence of noncondensable gas (nitrogen, through P_{pipe} values).

To study the effect of a possible influence of the sound velocity and noncondensable-gas desorption on the phenomenon, it was decided to perform also experiments after a lengthy pressurization (16-h minimum) of the liquid in the tank, assuming the pressurizing gas would have enough time to dissolve in the liquid. These criteria led to the test matrices, shown in Table 3, for each fluid and each pipe configuration.

IV. Results and Discussion

A. Reproducibility

To estimate the reproducibility of the phenomenon, it was decided to try to achieve three successful tests for each experimental configuration. For all configurations with ethanol and MMH as

Table 3 Test matrices

Hardware	Pressurization conditions	Short				Long
	Ethanol					
Straight and bent pipe	P_{tank}, MPa	2	2	2	2	2
	P_{pipe}, MPa	0.001	0.01	0.1	0.5	0.001
	Acetaldehyde					
Straight and bent pipe	P_{tank}, MPa	2	2	2	2	2
	P_{pipe}, MPa	0.001	0.03	0.1	0.5	0.001
	MMH					
Straight pipe	P_{tank}, MPa	2	——	2	2	——
	P_{pipe}, MPa	0.001	——	0.1	0.5	——
Bent pipe	P_{tank}, MPa	2	——	2	——	——
	P_{pipe}, MPa	0.001	——	0.1	——	——

fluids, the unsteady measurements related to waterhammer are shown in Figs. 3–9 with (from top to bottom) upstream pressure, downstream pressure, and temperature. On the timescale, $t = 0$ corresponds to the opening command of valve V7. Each curve corresponds to one experiment. These curves show that the reproducibility was excellent. The same excellent reproducibility was obtained with acetaldehyde. Not only was the overall shape similar for tests carried out under identical conditions, but sometimes the curves were even superimposed. Only the time of the waterhammer impact was not perfectly reproduced, but the maximum time lag was less than 5 ms from test to test. This discrepancy is probably due to the fact that the pneumatic system, operating the fast-opening valve V7, cannot perfectly produce the opening at a specified time.

B. Overall Waterhammer Characteristics

The main measurements for each successful test are shown in Tables 4–6, for ethanol, acetaldehyde, and MMH fluids. In these tables, in front of the name of the test, the following are listed successively: 1) the tank pressure; 2) the propellant temperature in the tank; 3) the sound velocity measurement in the tank with the ultrasonic device; 4) the initial pressure in the pipe; 5) the maximum pressure recorded on the upstream pressure transducer; 6) the maximum pressure recorded on the downstream pressure transducer (i.e., the waterhammer pressure); 7) the maximum propellant temperature recorded on the downstream thermocouple, T_{wh}; 8) the sound velocity in the pipe calculated from the upstream and downstream pressure records; and 9) the liquid front velocity calculated from the sound velocity and waterhammer pressure values.

All pressure values are absolute. The sound velocity in the pipe was calculated by dividing the distance between both pressure transducers by the propagation time of the waterhammer wave going back from the downstream transducer to the upstream one. Because of the complexity of these signals, it was not always easy to estimate this propagation time. We used characteristic peaks either from both upstream and downstream pressure curves and/or from the derivatives of these curves. Moreover, for the experiments with P_{pipe} equal to one and five atmospheres, the sound velocity in the pipe was not measured, because the smoothness of the waterhammer curves would have made the measurement very inaccurate. The final liquid

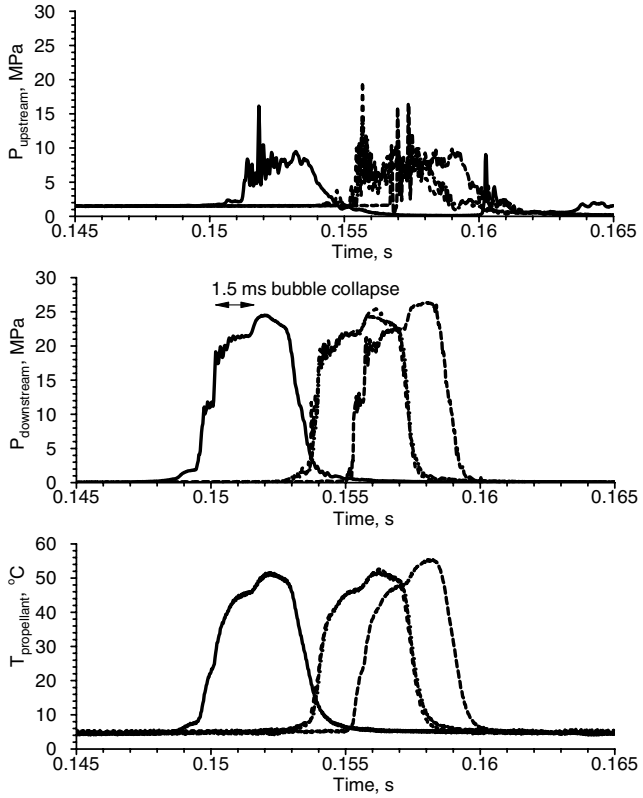

Fig. 3 Waterhammer unsteady measurements with ethanol, straight pipe, and vacuum pressure.

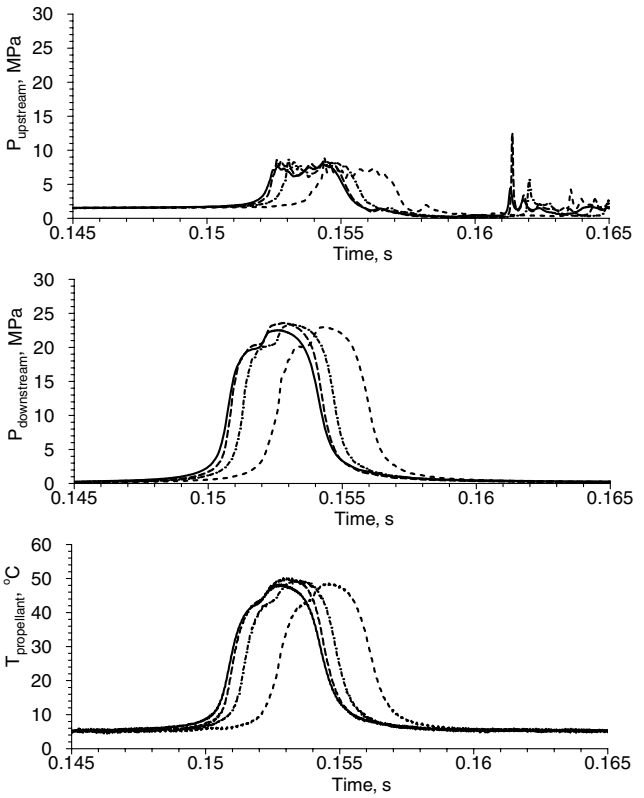

Fig. 4 Waterhammer unsteady measurements with ethanol, straight pipe, and 10-kPa pressure.

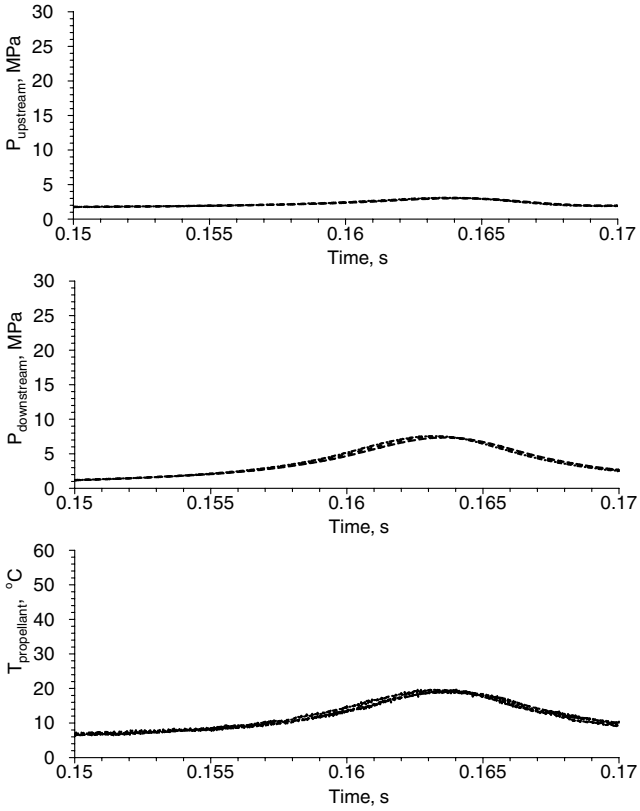

Fig. 5 Waterhammer unsteady measurements with ethanol, straight pipe, and 0.1-MPa pressure.

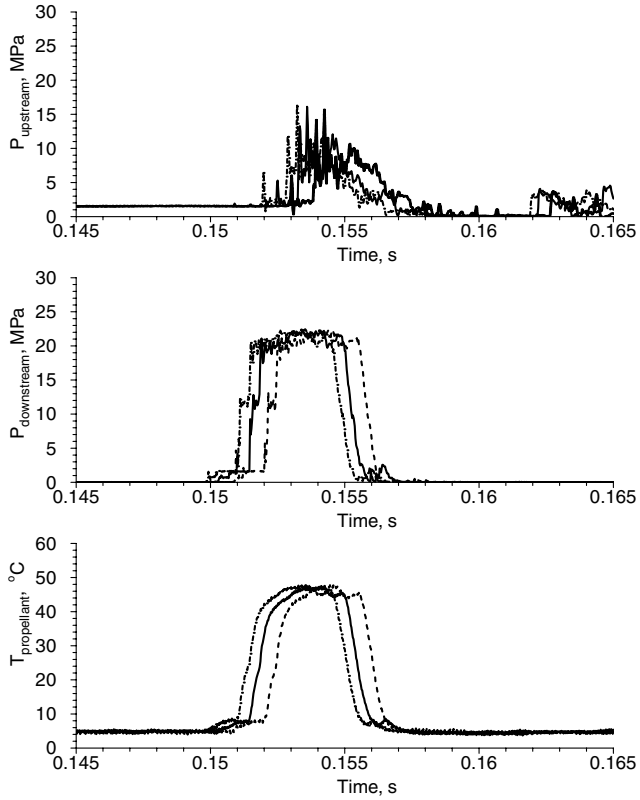

Fig. 6 Waterhammer unsteady measurements with ethanol, bent pipe, and vacuum pressure.

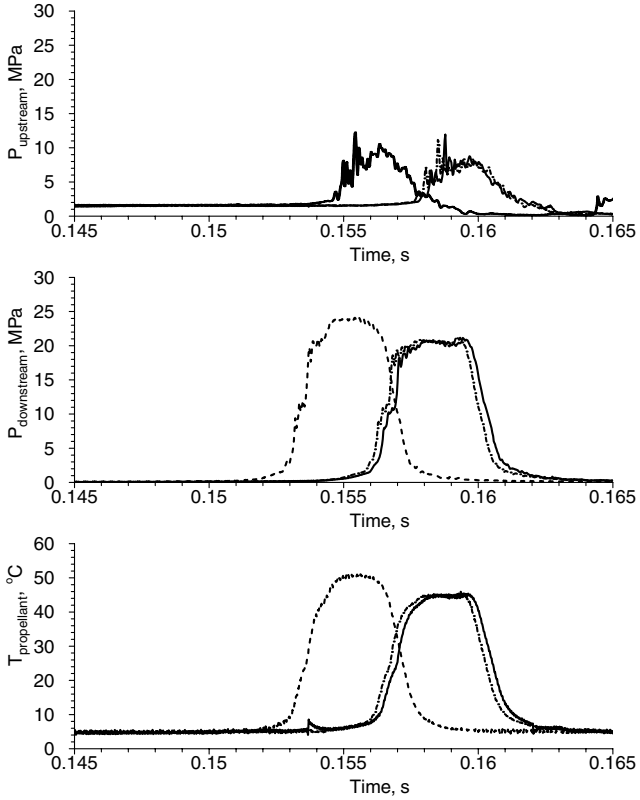

Fig. 7 Waterhammer unsteady measurements with ethanol, bent pipe, and 10-kPa pressure.

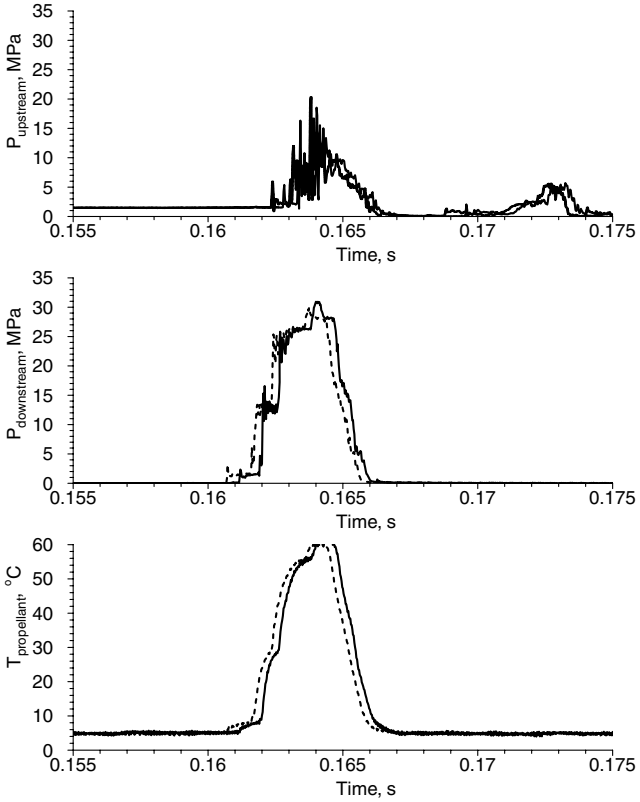

Fig. 8 Waterhammer unsteady measurements with MMH, straight pipe, and vacuum pressure.

front velocity was estimated from the classical waterhammer pressure expression:

$$P_{\text{wh}} = \rho_l \cdot c_s \cdot v_{l,f} \tag{2}$$

and will be compared with the liquid-front-velocity values, to be obtained in future CFD simulations. The validity of this estimation was demonstrated by velocity measurements in the measurement module in similar experiments [11] performed with the same setup.

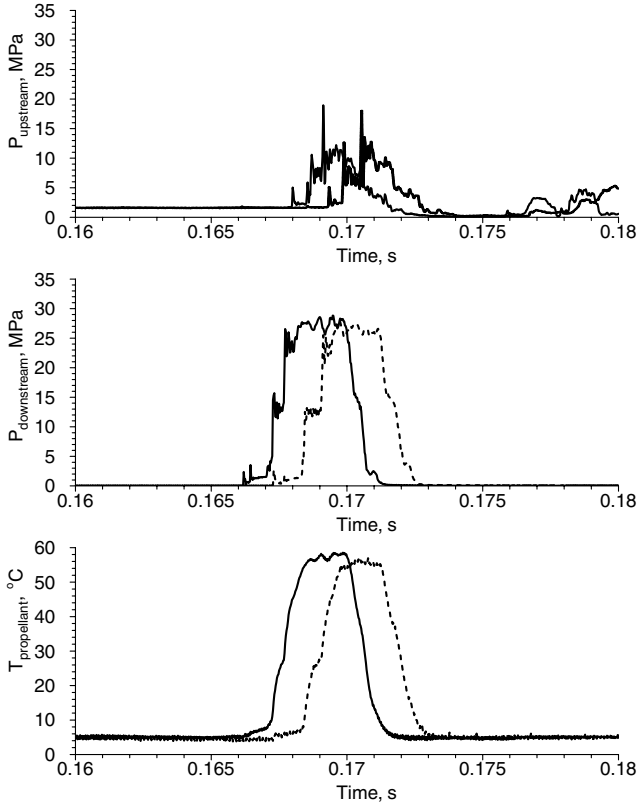

Fig. 9 Waterhammer unsteady measurements with MMH, bent pipe, and vacuum pressure.

1. Initial Conditions

Concerning the initial conditions of the experiments, the data in Tables 4–6 show that the tank pressure could be set close to around 2 MPa for all tests. Because the campaign was carried out in November and December, the propellant temperature in the tank was rather low, between 2 and 10°C. The mean sound velocity value measured for ethanol in the tank was about 1265 m/s. This value was slightly higher than the theoretical value of $\sqrt{K/\rho}$. Because the sound velocity was measured on a diameter of a cylindrical tank, this may be explained by the fact that the tank wall is cylindrical and the ultrasonic transducer is relatively wide (25 mm) compared with the internal tank diameter (135 mm). Therefore, the average distance traveled by the wave appears to be lower than the internal tank diameter due to the curved walls. For acetaldehyde, the mean measured value was 1150 m/s. No theoretical values were found in the literature. This was perhaps the first time this physical property has been measured for acetaldehyde. It should be noted that these values were not modified by the pressurization of the tank. The pressure did not affect the sound velocity value in the investigated range in any way. Likewise, no evolution of the sound velocity value was noticed after a lengthy pressurization of the fluids in the tank. For MMH, we did not manage to measure the sound velocity in the tank during the experimental waterhammer campaign because of a hardware failure. A measurement value of 1625 m/s was taken later at a higher MMH temperature and is close to the theoretical value at this temperature. Nevertheless, we shall see later that the MMH sound velocity value, measured in the pipe during the waterhammer experiments, is lower but close to the theoretical value. For the initial pipe pressure value, the vacuum corresponds to a pressure level lower than 1 kPa. Except for this vacuum value, which was obtained by pumping the pipe volume as much as possible, and for the atmospheric value, the other values (10 and 30 kPa) were difficult to

Table 4 Experimental characteristic results for ethanol tests

Test	P_{tank}, MPa	T_{tank}, °C	$c_{sound\ tank}$, m/s	P_{pipe}, MPa	$P_{upstream}$, MPa	P_{wh}, MPa	T_{wh}, °C	$c_{sound\ pipe}$, m/s	Computed $V_{liquid\ front}$, m/s
				Straight pipe[a]					
TDV_7	2.100	8	1294	Vacuum	19.8	25.6	53	1159	27.6
TDV_8	2.080	8	1294	Vacuum	14.1	24.5	52	1212	25.3
TDV_10	2.052	8	1279	Vacuum	16.6	26.4	55	1250	26.4
TDV_11	2.035	10	1271	Vacuum	16.2	24.6	55	1250	25.4
TDV_12[b]	1.980	5	1270	Vacuum	21.8	25.3	53	1230	25.7
TDV_13[b]	1.937	5	1270	Vacuum	15.6	25.1	53	1212	25.9
TDV_14[b]	2.029	5	1270	Vacuum	19.5	26.0	55	1230	26.4
$TD01_1$	1.990	10	1271	0.0090	9.0	23.1	49	1194	24.2
$TD01_2$	2.005	10	1271	0.0085	8.7	23.5	50	1194	24.6
$TD01_3$	2.017	10	1271	0.0090	12.6	23.7	50	1176	25.2
$TD01_4$	1.995	10	1271	0.0090	8.1	22.6	48	1212	23.4
$TD1_1$	2.033	8	1277	0.1	3.2	7.6	19	——	——
$TD1_2$	2.042	8	1277	0.1	3.2	7.7	20	——	——
$TD1_3$	2.032	8	1277	0.1	3.2	7.5	20	——	——
$TD5_1$	2.028	8	1277	0.50	2.2	2.6	9	——	——
$TD5_2$	2.021	8	1277	0.50	1.6	2.7	9	——	——
$TD5_3$	2.015	8	1277	0.57	1.5	2.7	9	——	——
				Bent pipe[c]					
TCV_1	2.003	11	1256	Vacuum	15.8	22.5	48	1229	22.9
TCV_3	2.026	11	1256	Vacuum	16.6	22.6	49	1212	23.3
TCV_4	2.006	11	1256	Vacuum	16.6	22.5	47	1229	22.8
TCV_5[b]	2.002	7	1255	Vacuum	16.5	22.8	48	1229	23.2
TCV_6[b]	2.132	7	1255	Vacuum	16.4	23.9	50	1229	24.3
TCV_7[b]	2.083	7	1255	Vacuum	15.2	23.6	50	1229	24.0
$TC01_1$	2.112	7	1255	0.0092	12.4	24.3	51	1248	24.3
$TC01_2$	1.992	7	1255	0.0096	11.3	21.4	46	1248	21.4
$TC01_3$	1.972	7	1255	0.0097	12.0	21.2	45	1212	21.9
TC_1	2.001	11	1256	0.1	3.0	6.4	17	——	——
TC_2	2.012	11	1256	0.1	3.0	7.0	18	——	——
TC_3	2.028	11	1256	0.1	3.1	7.0	19	——	——
$TC5_1$	2.001	11	1243	0.52	2.2	2.6	9	——	——
$TC5_2$	1.996	11	1243	0.50	2.2	2.6	9	——	——
$TC5_3$	2.023	11	1243	0.49	2.2	2.6	10	——	——

[a]TDx_01 is the first straight-pipe test, with $x = V$ for the vacuum or pressure value (atm).
[b]Test performed after a long pressurization of the tank (greater than 16 h).
[c]TCx_01 is the first bent-pipe test, with $x = V$ for the vacuum or pressure value (atm).

Table 5 Experimental characteristic results for acetaldehyde tests

Test	P_{tank}, MPa	T_{tank}, °C	$c_{sound\ tank}$, m/s	P_{pipe}, MPa	$P_{upstream}$, MPa	P_{wh}, MPa	T_{wh}, °C	$c_{sound\ pipe}$, m/s	Computed $V_{liquid\ front}$, m/s
					Straight pipe[a]				
TDV_1	2.017	6	1150	Vacuum	20.1	27.2	57	1143	30, 5
TDV_2	1.985	6	1150	Vacuum	20.9	28.2	58	1127	32, 1
TDV_3	2.023	6	1150	Vacuum	18.7	28.9	59	1143	32, 4
TDV_4	2.000	6	1150	Vacuum	19.7	27.5	58	1143	30, 9
TDV_5[b]	2.016	6	1154	Vacuum	20.1	27.6	58	1143	30, 9
TDV_7[b]	2.110	6	1154	Vacuum	21.1	28.1	59	1159	31, 1
TDV_8[b]	2.065	6	1154	Vacuum	18.4	27.7	58	1127	31, 5
$TD03_2$	1.970	6	1150	0.0259	18.8	26.9	58	1143	30, 2
$TD03_3$	2.026	6	1150	0.0255	17.6	27.4	59	1143	30, 7
$TD03_4$	2.047	6	1150	0.0307	19.7	27.7	59	1159	30, 6
$TD1_1$	2.025	6	1150	0.1	1.4	6.0	17	——	——
$TD1_2$	2.017	6	1150	0.1	1.4	6.8	18	——	——
$TD1_3$	2.012	6	1150	0.1	1.4	6.3	17	——	——
$TD5_1$	2.034	6	1150	0.52	1.4	3.1	10	——	——
$TD5_2$	2.025	6	1150	0.48	1.3	3.1	11	——	——
$TD5_3$	2.032	6	1150	0.48	1.4	3.1	10	——	——
					Bent pipe[c]				
TCV_1	1.993	6	1147	Vacuum	16.7	22.9	48	1145	25, 6
TCV_2	2.007	6	1147	Vacuum	17.5	22.9	49	1161	25, 3
TCV_3	2.014	6	1147	Vacuum	17.0	23.2	49	1161	25, 6
TCV_4[b]	1.997	5	1160	Vacuum	15.5	22.8	49	1145	25, 5
TCV_5[b]	2.086	5	1160	Vacuum	17.2	23.7	50	1177	25, 8
TCV_6[b]	2.068	5	1160	Vacuum	18.2	23.8	50	1161	26, 2
$TC03_1$	2.023	6	1147	0.0276	11.5	21.2	46	1145	23, 8
$TC03_2$	1.962	6	1147	0.0250	9.7	19.6	44	1145	22, 0
$TC03_3$	2.000	6	1147	0.0238	9.7	20.1	44	1161	22, 2
TC_1	1.992	6	1147	0.1	3.7	9.6	24	——	——
TC_2	2.019	6	1147	0.1	3.4	8.6	22	——	——
TC_3	2.026	6	1147	0.1	3.7	9.9	25	——	——
$TC1_4$	2.036	6	1147	0.1	3.4	8.8	22	——	——
$TC5_1$	2.001	4	1147	0.52	2.2	2.9	10	——	——
$TC5_3$	1.984	4	1147	0.50	2.2	2.8	9	——	——
$TC5_3$	1.999	4	1147	0.49	2.2	2.8	10	——	——

[a]TDx_01 is the first straight-pipe test, with $x = V$ for the vacuum or pressure value (atm).
[b]Test performed after a long pressurization of the tank (greater than 16 h).
[c]TCx_01 is the first bent-pipe test, with $x = V$ for the vacuum or pressure value (atm).

Table 6 Experimental characteristic results for MMH tests

Test	P_{tank}, MPa	T_{tank}, °C	$c_{sound\ tank}$, m/s	P_{pipe}, MPa	$P_{upstream}$, MPa	P_{wh}, MPa	T_{wh}, °C	$c_{sound\ pipe}$, m/s	Computed $V_{liquid\ front}$, m/s
					Straight pipe[a]				
TDV_2	2.004	3	——	Vacuum	20.5	30.1	60	1455	23.4
TDV_3	2.012	3	——	Vacuum	18.6	31.0	63	1481	23.7
$TD1_1$	2.002	3	1625[b]	0.1	2.9	6.8	18	——	——
$TD1_2$	2.001	3	——	0.1	2.9	7.0	19	——	——
$TD5_1$	1.960	3	——	0.434	2.0	2.4	9	——	——
					Bent pipe[c]				
TCV_1	2.095	2	——	Vacuum	18.2	27.9	57	1493	21.1
TCV_2	2.012	2	——	Vacuum	19.1	28.9	59	1493	21.9
TC_1	1.992	2	1625[b]	0.1	2.8	6.1	17	——	——
TC_2	2.019	2	——	0.1	2.8	6.4	17	——	——

[a]TDx_01 is the first straight-pipe test, with $x = V$ for the vacuum or pressure value (atm).
[b]Measured in the tank after the test campaign with MMH temperature at 13°C.
[c]TCx_01 is the first bent-pipe test, with $x = V$ for the vacuum or pressure value (atm).

set accurately because it took too long to open and close the adjusting valve. However, the obtained settings were not far from the targeted values.

2. *Waterhammer Results*

In Tables 4–6 (respectively, for ethanol, acetaldehyde, and MMH), the maximum value P_{wh}, measured on the downstream pressure transducer, shows that the waterhammer amplitude decreases when P_{pipe} increases. The decrease is small when P_{pipe} varies between a vacuum and 10 kPa (i.e., under or above the fluid vapor pressure). The decrease was great for $P_{pipe} = 0.1$ MPa and there was no waterhammer for $P_{pipe} = 0.5$ MPa. The values of T_{wh} evolved similarly, depending on P_{pipe}. The maximum temperatures can reach high values (up to about 60°C). These temperature peaks in the liquid can be theoretically reproduced by applying isentropic compression of the NCG and taking into account the presence of phase changes near the liquid front. Indeed, though it was not possible to visually inspect the moving liquid front with the present configuration, the pressure condition in the pipe was well below the vapor line under vacuum conditions or crossed the vapor line during the transient once the initial pressure was greater than the vapor pressure (Fig. 10). This meant that the front was boiling from the start (vacuum) or later (larger initial pipe pressures), resulting in a local two-phase mixture of vapor and liquid. Meanwhile, the NCG present in the pipe was compressed when the front was traveling downstream

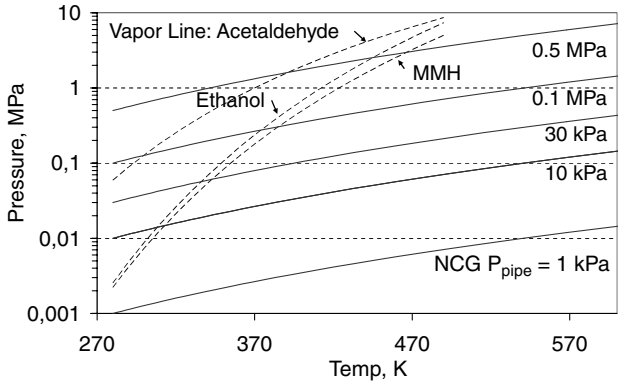

Fig. 10 Calculated adiabatic pressure and temperature evolution of the NCG for various initial pipe pressures along with vapor lines of ethanol, acetaldehyde, and MMH (straight pipe).

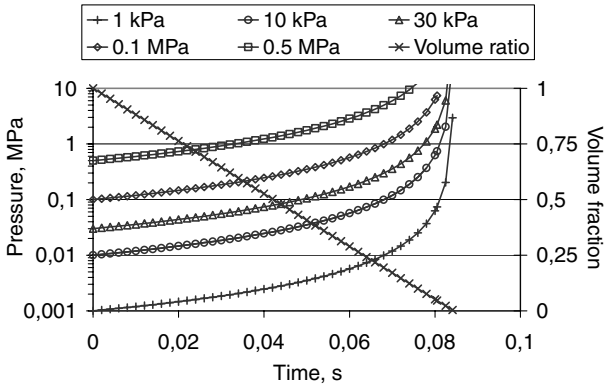

Fig. 11 Calculated adiabatic pressure and volume fraction for the NCG (i.e., N_2) as a function of time for the straight pipe.

toward the pipe end (Fig. 11). Because this compression occurs very fast (between 85 ms, assuming a final front velocity of 25 m/s, and 150 to 170 ms, based on the experimental values) it is primarily adiabatic at its boundaries (i.e., end plug and pipe walls), but has an intense mixing and heat transfer at the multiphase liquid-NCG front. A pure adiabatic compression of the NCG, that is,

$$P_1 \cdot V_1^{\gamma} = P_2 \cdot V_2^{\gamma} \quad \text{with } V_2 = V_1 - A v_{f,l} \Delta t \tag{3}$$

would result in a very high temperature (greater than 2500 K) being reached, assuming ideal gas properties. This means that the critical temperature was crossed, occurring roughly at about 66 and 61 ms for ethanol and acetaldehyde, respectively. The finite velocity of the two-phase front impacting the pipe end resulted in an intense mixing of the NCG with the liquid and a resulting intense heat transfer between the NCG and the liquid. Because of a density and a specific heat capacity ratio for acetaldehyde of about 22 and 2.37, respectively, between both liquid and NCG in the remaining compression volume, the corresponding temperature for perfect mixing rises in the liquid is given by

$$m_g C_{p,g}(T_g - T_{\text{eq}}) = m_l C_l (T_{\text{eq}} - T_l) \tag{4}$$

or

$$T_{\text{eq}} = \frac{\alpha T_g + T_l}{\alpha + 1} \quad \text{with } \alpha = \frac{\rho_g C_{p,l}}{\rho_l C_l} \tag{5}$$

The computed temperature increase is about 46 K if P_{wh} rises to about 28.9 MPa. For lower values of 6.6 and 3.1 Mpa, this results in a ΔT of 10 and 4.5 K. This $\Delta T = T_{\text{wh}} - T_{\text{tank}}$ appears to correspond very well with the measured data in Tables 4–6.

Though the pressure of 10 kPa is greater than the ethanol vapor pressure and 30 kPa is less than the acetaldehyde vapor pressure, the evolution of the waterhammer pressure vs the initial pipe pressure did not illustrate any discrete changes in the pressure peak values. Hence, the vapor pressure value is not important for the pressure rise tendency.

For ethanol and acetaldehyde, the sound velocity values calculated from the pressure measurements in the pipe were close to those measured in the tank and close to the theoretical value in thin pipes (1187 m/s). They may even be considered to be identical for acetaldehyde. This means that two-phase flow effects, cavitation, NCG absorption, desorption and bubbles have no influence on this aspect of the phenomenon when P_{pipe} values are lower than 0.1 MPa. Comparing the waterhammer characteristics P_{wh} and T_{wh} according to the fluids in Tables 4–6, the results for ethanol and acetaldehyde are confusing. From the straight-pipe experiments at P_{pipe} values lower than 0.1 MPa, and from the bent-pipe experiment at vacuum, P_{wh} and T_{wh} values were higher for acetaldehyde than for ethanol. Because the sound velocity values were close to each other, this implies that the liquid front velocities in the pipe were higher for acetaldehyde than for ethanol: about 31 vs 26 m/s for straight-pipe results (TDV) and 25 vs 23 m/s for bent-pipe results (TCV). This can be attributed to the lower viscosity value of acetaldehyde, which is one order of magnitude lower than that of ethanol, and, to a lesser extent, to a lower mass density value (see Table 2). The straight pipe at 0.1 MPa clearly yielded opposite results regarding P_{wh}. Though the final P_{wh} was close to the critical pressure, the initial pressure level was well above the vapor pressure for ethanol and close to that for acetaldehyde. During the wave travel, the ethanol front boiled at a much later stage (approximately 44 ms) than the acetaldehyde front (13 ms). This boiling front, which was more intense for the latter one due to the longer exposure time, possibly slows down the front velocity more explicitly than the rise due to the lower viscosity, resulting in a less intense waterhammer. For the 0.5 MPa case, the point of boiling occurred for both fluids closer in time (respectively, 58 and 48 ms), because there was a smaller differential frontal velocity change. It is rather difficult to comment on the results for the bent pipe at 10 kPa (ethanol) vs 30 kPa (acetaldehyde) due to the different initial pressures and their opposite relative position from the vapor curve.

At low P_{pipe} values (vacuum), the waterhammer was stronger for MMH than for ethanol, which can be easily explained by the very high value of the sound velocity (about 1600 m/s in the tank and 1480 m/s in the pipe) for MMH. But at an atmospheric P_{pipe} value, the waterhammer was weaker for MMH than for ethanol. This result could not be explained. The discrepancy between the values measured during the MMH waterhammer experiments ($\sim$1500 m/s) and the value measured in the tank with the ultrasonic transducer ($\sim$1600 m/s), may be explained by the pipe wall elasticity: the theoretical value is 1452 m/s. In addition, it is assumed that because the waterhammer amplitude with MMH was higher than with the inert fluids, this might indicate the presence of a slight fluid–structure interaction.

No matter what the fluid, P_{wh} and T_{wh} were lower for the bent pipe than for the straight pipe. This sounds logical, because it seems natural that the kinetic energy of the fluid is lost in the bend, but it would appear that this decrease in P_{wh} was partially compensated for by a higher value of the sound velocity in the bent pipe, which we are unable to explain.

Finally, at low P_{pipe} values, the waterhammer amplitude with MMH can be extrapolated from the ethanol amplitude by multiplying the latter value by the ratio of the sound velocity, with an accuracy of about 5%.

3. *Description of the Evolving Waterhammer Pressure*

Considering the pressures recorded at the pipe end plug ($P_{\text{downstream}}$ from Figs. 3–9) and the same measurements for acetaldehyde, as long as P_{pipe} values are low enough (i.e., below 0.1 MPa), the pressure evolution at the downstream transducer

always has the same complex shape, shown in Fig. 12, for straight and bent pipes.

The first obvious comment is that the phenomenon is not exactly the same for each pipe configuration. For the straight pipe, there is a small growth (indicated as "bump" in Fig. 12) at the end of the waterhammer, which does not occur for the bent pipe. Before this event, the generation of the waterhammer followed the same scenario for both hardware configurations. First, a small pressure increase occurred because of the arrival of the liquid front over the pressure transducer and because of the filling of the internal volume of the measurement module (Fig. 2), between this transducer and the end plug. This was followed by a first large increase in pressure with a steep gradient, interrupted by a first plateau. As discussed before, this first jump results from an adiabatic compression of the residual noncondensable gas (1 kPa for vacuum tests, 10 or 30 kPa for the others) because calculations have shown that such a steep pressure increase (18 MPa/ms) can be obtained with the adiabatic compression of gas in the measurement module ($\sim$1450 mm^3). After the plateau, another jump of pressure occurred through a second steep slope, to reach a second plateau. This would be the actual waterhammer. Finally, there was a progressive building of a pressure plateau. According to the test, the level of this plateau above the second plateau is more or less pronounced. This progressive increase in pressure at the end of the waterhammer plateau was apparent at lower initial pipe pressures. The vapor bubbles caused by the boiling process at the front probably take a finite time to collapse and hence increase the pressure further toward its final value, with a characteristic time delay. Based on the Rayleigh–Plesset equation for bubble collapse rate [12], the characteristic time τ of an exponential bubble collapse can be estimated by

$$\frac{1}{\tau} = C_c \frac{V_{\text{ch}}}{\sigma} \rho_{\text{vap}} \sqrt{\frac{2}{3} \frac{P - P_{\text{vap}}}{\rho_l}} \tag{6}$$

where C_c and V_{ch} are the phase rate coefficient and the characteristic velocity, respectively, set at 0.01 and 4 m/s, taken from practical investigations [13]. If the surface tension and the vapor density are set to 0.0063 N/m and 0.72 kg/m^3 corresponding to T_{wh}, the characteristic time at the waterhammer pressure value corresponds to 1.5 ms. This corresponds quite well with the time delay seen in Fig. 3 for the pressure rise after the end plateau. In the case of the bent pipe, this plateau was ended by a large steep decrease of the pressure down to the vacuum. In the case of the straight pipe, there was a small increase (indicated as "bump" in Fig. 12) before a similar pressure decrease occurred. This ended with the waterhammer wave passing over the pressure transducer. Along the entire curve, there were small high-frequency oscillations.

This evolution in pressure, with a multiple step increase to reach the maximum waterhammer pressure value, is surprising. It may be due to two-phase flow phenomena, because for intermediate P_{pipe} values between vacuum and atmosphere, the pressure evolution is often smoothed so that these steps are less apparent (Figs. 5 and 7).

It should be noted that this pressure evolution occurred irrespective of the fluid used. Only the MMH curves revealed a small peak at the beginning of the small growth for straight-pipe tests and several peaks during the plateau phase for bent-pipe tests. This means that inert fluids can be used instead of actual propellants, at least ethanol instead of MMH, to investigate the waterhammer phenomenon.

Then the temperatures recorded at the same location, $T_{\text{propellant}}$ from Figs. 3–9, show that the fluid temperature follows a rather strict parallel evolution to the pressure under all experimental conditions. As has already been described, this fast process could be described as an adiabatic compression of the pressurizing gas that, due to intense mixing at the liquid interface, was transferred to the liquid. These temperature records should be useful to check the validity of the two-phase flow models in the waterhammer simulations.

Finally, the pressures recorded upstream from the tested pipes (P_{upstream} from Figs. 3–9) reveal a complex structure. This is probably due to the transducer being installed in a recess and to the partial reflection of the pressure wave traveling toward the tank through the numerous section changes in the valves and in the feed line upstream from the tested pipe. Such phenomena were not considered in the present study. These pressure records were only used to measure the sound velocity in the fluid during the experiment, to check this value with the results of the future CFD simulations.

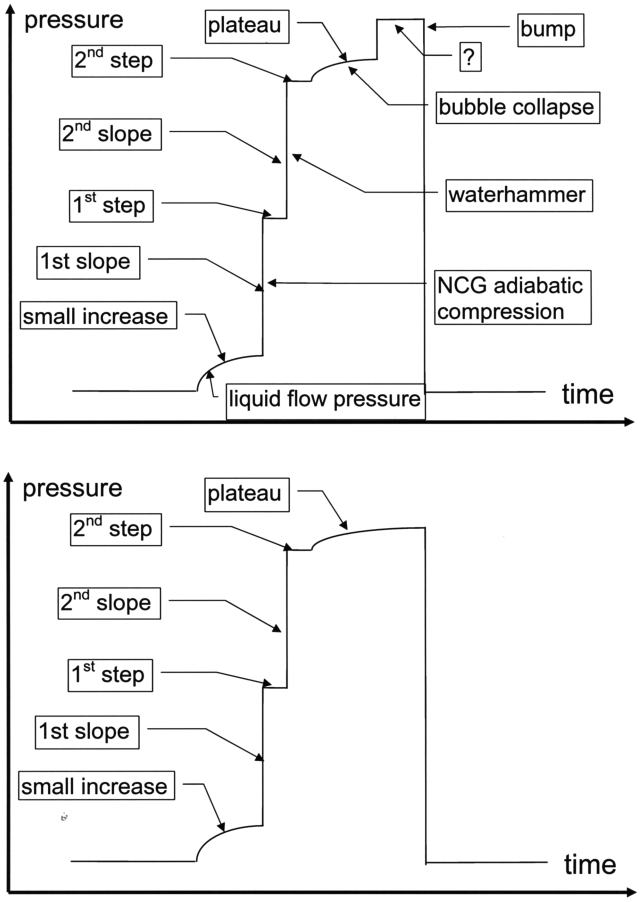

Fig. 12 Schematics of the waterhammer pressure evolution according to hardware (top: straight pipe and bottom: bent pipe) for low P_{pipe} pressures.

V. Conclusions

Because the literature has not provided well-documented experiments reproducing all the possible two-phase flow phenomena resulting from waterhammer in satellite or spacecraft propulsion systems, a dedicated simplified experiment was designed and performed. This experiment showed that at low P_{pipe} values, the time evolution of the waterhammer pressure has a complex structure, most of which, but not all, could be interpreted without further experimental evidence. Accurate measurements obtained with experiments with well-known and well-defined initial and boundary conditions are now available. These measurements are going to be used in the near future to improve and validate two-phase flow models such as cavitation, condensation, and noncondensable-gas absorption and desorption in a CFD solver. This solver should enable waterhammer evaluation during the design of rocket propulsion feed systems. It is also hoped that numerical simulations will make it possible to fully explain the complex structure of the waterhammer phenomenon in the present experiments.

The results have also demonstrated that ethanol can be used as a replacement fluid instead of the currently used toxic MMH propellant. The fluid behaviors are identical and the amplitudes can be deduced from one fluid to the other by means of the sound velocity ratio.

Acknowledgments

The authors would like to thank ESA European Space Research and Technology Centre (ESTEC) for its financial support, Centre National d'Etudes Spatiales (CNES) for its cooperation, and Alcatel Space for the loan of the quick valve and pipes.

References

[1] Tijsseling, A. S., "Fluid-Structure Interaction in Liquid-Filled Pipe Systems: A Review," *Journal of Fluids and Structures*, Vol. 10, Feb. 1996, pp. 109–146. doi:10.1006/jfls.1996.0009

[2] Wiggert, D. C., and Tijsseling, A. S., "Fluid Transients and Fluid-Structure Interaction in Flexible Liquid-Filled Piping," *Applied Mechanics Reviews*, Vol. 54, Sept. 2001, pp. 455–481. doi:10.1115/1.1404122

[3] Bergant, A., Simpson, A. R., and Tijsseling, A. S., "Water Hammer with Column Separation: A Historical Review," *Journal of Fluids and Structures*, Vol. 22, 2006, pp. 135–171. doi:10.1016/j.jfluidstructs.2005.08.008

[4] Fan, D., and Tijsseling, A. S., "Fluid-Structure Interaction with Cavitation in Transient Pipe Flows," *Journal of Fluids Engineering*, Vol. 114, No. 2, 1992, pp. 268–294.

[5] Tijsseling, A. S., Vardy, A. E., and Fan, D., "Fluid-Structure Interaction and Cavitation in a Single-Elbow Pipe System," *Journal of Fluids and Structures*, Vol. 10, May 1996, pp. 395–420. doi:10.1006/jfls.1996.0025

[6] Vardy, A. E., Fan, D., and. Tijsseling, A. S., "Fluid-Structure Interaction in a T-Piece Pipe," *Journal of Fluids and Structures*, Vol. 10, Oct. 1996, pp. 763–786. doi:10.1006/jfls.1996.0052

[7] Holmboe, E., and Rouleau, W. T., "The Effect of Viscous Shear on Transients in Liquid Lines," *Journal of Basic Engineering*, Vol. 89, No. 1, 1967, pp. 174–180.

[8] Swaffield, J., "The Influence of Bends on Fluid Transients Propagated in Incompressible Pipe Flow," *Proceedings of the Institution of Mechanical Engineers*, Vol. 183, Pt. 1, No. 29, 1968, pp. 603–614.

[9] Driels, M. R., "An Investigation of Pressure Transients in a System Containing a Liquid Capable of Air Absorption," *Journal of Fluids Engineering*, Vol. 28, Sept. 1973, pp. 408–414.

[10] Elansary, A., Silva, W., and Chaudry, M., "Numerical and Experimental Investigation of Transient Pipe Flows," *Journal of Hydraulic Research*, Vol. 32, No. 5, 1994, pp. 689–706.

[11] Gibek, I., and Maisonneuve, Y., "Waterhammer Tests With Real Propellants," AIAA Paper 2005-4081, 2005.

[12] Brennen, C., *Cavitation and Bubble Dynamics*, Oxford Univ. Press, Oxford, 1995.

[13] Athavale, M. M., Li, H. Y., Jiang, Y., and Singhal, A. K., "Application of the Full Cavitation Model to Pumps and Inducers," *International Journal of Rotating Machinery*, Vol. 8, No. 1, 2002, pp. 45–56. doi:10.1155/S1023621X02000052

D. Talley
Associate Editor